Electronic Supplementary Information for Amine-Ligand Modulated Ruthenium as a Superior Bi-functional Hydrogen Electrocatalyst in Alkaline Media

Jie Wang,[a] Jing Liu,*[a] Boyang Zhang,[a] Jie Gao,[a] Guangbo Liu,[a] Xuejing Cui,[a] Jin-xun Liu,*[b] Luhua Jiang*[a]

[a] College of Materials Science and Engineering, Qingdao University of Science and Technology, Qingdao, Shandong 266042, China

[b] Department of Chemical Physics, University of Science and Technology of China, Hefei, Anhui 230026, China

* Corresponding authors:

E-mail: liuj955@qust.edu.cn (J. Liu);

jxliu86@ustc.edu.cn (J. Liu);

luhuajiang@qust.edu.cn (L. Jiang)

Table of Contents

Supplementary Experimental section

Materials. Ruthenium (III) chloride hydrate ($RuCl_3 \cdot 3H_2O$, Tianjin Maisike Chemical Co., Ltd. ≥ 37%), sodium hydroxide (NaOH, Sinopharm Chemical Reagent Co. Ltd. ≥ 96%) Ethylene Glycol ($C_2H_6O_2$, Sinopharm Chemical Reagent Co. Ltd. ≥ 99.8%), trisodium citrate dihydrate ($C_6H_5Na_3O_7 \cdot 2H_2O$, Sinopharm Chemical Reagent Co. Ltd. ≥ 98%), polyethylene imine (Sigma-Aldrich Co., Mw 25000), hydrochloric acid (HCl, Yantai Far Eastern Fine chemical Co. Ltd.), ethanol absolute (CH_3CH_2OH, Sinopharm Chemical Reagent Co. Ltd. ≥ 99.8%), potassium hydroxide (KOH, Sinopharm Chemical Reagent Co. Ltd. ≥85%), Sodium Chloride (NaCl, Sinopharm Chemical Reagent Co. Ltd. ≥ 99.8%) and Nafion® 117 solution (Sigma-Aldrich Co., 5.wt.%) were used as received without any further purification.

Modification of Carbon black XC. Vulcan XC was firstly subjected to acidic treatment by refluxing in 5 M HNO_3 at 120^{o}C for 6 h. The precipitate was collected and washed to pH=7 by copious of deionized water. After dried in an oven at 120^{o}C for 8 h, the carbon black was obtained to use as the support and denoted as XC. For PEI modification, typically, 500 mg of XC were dispersed homogenously in different concentrations of PEI aqueous solution, i. e. 1 wt.%, 5 wt.% and 10 wt.%, respectively. The mixture was then stirred magnetically at ambient for 8 h. After that, the black powder was filtrated, washed by deionized water and then dried. The obtained carbon black was denoted as SPEI-XC, PEI-XC, and LPEI-XC.

Physical characterization. The crystalline structure of the catalysts was studied on a Rigaku D/MAX/2500PC X-ray diffractometer with a Cu K_α radiation source (=0.154 nm) with a scan rate of 5^o min^{-1} from 15^o to 80^o. The morphology of the catalysts was characterized on a JEM-2100PLUS transmission electron microscopy (TEM) equipped with energy dispersive X-ray Spector (EDS). Fourier Transform infrared spectroscopy (FTIR) was conducted to identify the functional groups in the catalyst. The elemental composition and surface chemical states were probed by X-ray photo electron spectroscopy (XPS) on AXIS SUPRA spectrophotometer. Inductively coupled plasma optical emission spectroscopy (ICP-OES) was carried out on an Agilent 5110 spectrometer.

Electrochemical Characterization. The electrochemical properties of the catalysts were investigated by a three-electrode system using a rotating disk electrode. The potential was controlled by a potentiostat (Pine Instrument). A radiometer speed control unit and a rotating disk electrode radiometer from pine instrument company were used. A diameter of 5mm glassy carbon (GC) electrode, a graphite rod and Mercury/Mercury oxide (Hg/HgO) electrode were

employed as working electrode, counter electrode and reference electrode, respectively. All the potentials in the work were calibrated to reversible hydrogen electrode (RHE). No iR compensation was used in this study. The catalyst ink was prepared by dispersing 5 mg of catalyst in 2 mL of ethanol for 15 min ultra-sonication. After that, 30 μL of 5 wt.% Nafion solution was added and ultra-sonicated for 15 min. Then, 20 μL of ink was drop-casted on the GC electrode. The carbon supported catalyst loading on the GC is 255 μg_{cat} cm^{-2}_{geo}. A 20%Pt/C purchased from Johnsen Mattery Co. is used as the benchmark with a loading of 20.4 μg_{Pt} cm^{-2}_{geo} on the electode. The catalyst modified electrode was firstly experienced a surface cleaning process by cyclic voltametric scanning in the potential range from 0 to 0.1 V_{RHE} with a scan rate of 50 mV s^{-1} for 30 cycles. After that, Cyclic voltammetry (CV) curves of the catalysts were recorded in N_2-saturated 0.1 M KOH with a scan rate of 10 mV s^{-1}. The hydrogen oxidation reaction was tested in H_2 saturated 0.1 M KOH with a scan rate of 1 mV s^{-1}. The HOR polarization curves was collected from -0.004 V_{RHE} to 0.25 V_{RHE} at rotating rates of 2500 rpm, 1600 rpm, 900 rpm and 400 rpm, respectively. The kinetic current densities were determined by plotting the reciprocal of current density against $\omega^{-1/2}$ based on the Koutecky-Levich equation. Subsequently, linear sweep voltammetry (LSV) curves from -0.05 V_{RHE} to 0.05 V_{RHE} with a scan rate of 1 mV s^{-1} were recorded in the H_2-saturated 0.1 M KOH electrolyte. The corresponding Tafel plots were then derived. The kinetic parameter, Exchange current density (J_o), could be deduced by extrapolating the linear segments of anodic and cathodic branch of Tafel plots. Chronoamperometry test was conducted at potential of 0.1 V_{RHE} in H_2 saturated 0.1 M KOH with a rotating rate of 400 rpm. Accelerated degradation tests (ADT) were performed by cyclic voltametric scanning from -0.004 V_{RHE} to 0.25 V_{RHE} with a scan rate of 100 mV s^{-1} for 1000 cycles in H_2-saturated 0.1 M KOH. The electrochemical active surface area (ECSA) of Ru catalysts for HOR was calculated from underpotential deposition (UPD) of copper (Cu) ($Cu_{upd)}$ stripping method. The background CV curves were firstly tested in N_2 saturated 0.5 M H_2SO_4 from 0 to 0.675 V_{RHE} at 10 mV s^{-1}. Then, the Cu underpotential deposition is carried out at 0.266 V_{RHE} for 100 s in N_2 saturated 0.5 M H_2SO_4 electrolyte containing 5 mM $CuSO_4$. After that, the Cu stripping curves were recorded from 0.266 V_{RHE}

to 0.675 V_{RHE} with a scanning rate of 10 mV s^{-1}. ECSA for Ru catalysts were calculated by the following equation

$$ECSA = \frac{area(Cu_{upd})/\upsilon}{0.42mC\ cm^{-2} \cdot M_{Ru}}$$

Where area (Cu_{upd}) is the integrated area in Cu stripping curves and the background CV curves, υ is the scanning rate, 0.42 mC cm^{-2} is the specific capacity of monolayer Cu_{upd}, M_{Ru} is the mass of Ru on the electrode.

The hydrogen evolution reaction (HER) was tested in H_2 saturated 1M KOH, 0.1M KOH and 0.6 M (3.5 wt.%) NaCl with a scan rate of 1 mV s^{-1}, respectively. Before recording the HER polarization curves, the electrode was subjected to CV cycling between 0.01 to -0.10 V_{RHE} with a scan rate of 50 mV s^{-1} for 30 cycles in N_2-saturated electrolyte. The durability test for HER were conducted by steady potential and ADT protocols. The potential is selected according to the HER current density at -10 mA cm^{-2}. In 1 M KOH, the electrode was held at a steady potential of -0.02 V_{RHE} for 12 h, which was held at -0.1 V_{RHE} and -0.354 V_{RHE} in 0.1 M KOH and 0.6 M NaCl, respectively. The ADT is taken by CV scanning for 1000 cycles with 100 mV s^{-1} from 0.01 V to -0.1 V_{RHE} in 1 M KOH. The potential window is set from 0.01V_{RHE} to -0.25 V_{RHE} for 0.1 M KOH and 0.112 V_{RHE} to -0.412 V_{RHE} for 0.6 M NaCl. The ECSA of the catalyst for HER is estimated by capacity currents at different scanning rates. [1] In N_2 saturated 1 M KOH, CV curves were recorded between 0.2-0.3 V_{RHE} at scanning rates of 20 mV s^{-1}, 40 mV s^{-1}, 60 mV s^{-1}, 80 mV s^{-1} and 100 mV s^{-1}, respectively. The catalyst loading on GC electrode is 255 $\mu g_{cat} cm^{-2}$ for Ru-based catalysts and Pt/C.

Calculation of active sites. Cu_{upd} was used to calculate the active sites of the Ru/PEI-XC and other comparative Ru based samples. In this method, the number of active sites (n) can be calculated based on the UPD copper stripping charge (Q_{Cu}, $Cu_{upd} \rightarrow Cu^{2+}+2e^{-}$) using the following equation.

$$n = \frac{Q_{Cu}}{2 \cdot F}$$

where F is the Faraday constant (96,485.3 C mol^{-1})

The TOF (s^{-1}) was calculated by the following formula.[2]

$$TOF(s^{-1}) = \frac{I}{2 \cdot F \cdot n}$$

where I is the current (A) during linear sweep voltammetry (LSV), F is the Faraday constant (96,485.3 C mol^{-1}), n is the number of active sites (mol). The factor 1/2 is based on the assumption that two electrons are necessary to form one hydrogen molecule.

Density functional theory (DFT) calculations. All DFT calculations were performed using projector augmented wave (PAW)[3] potentials and the Perdew-Burke-Ernzerhof (PBE) functional[4] as implemented in the Vienna Ab initio Simulation Package (VASP) [5, 6] . The cutoff energy for the plane wave basis was specified by 400 eV. All the DFT calculations were performed on a p (2×2) slab model of Ru (0001) surface, with the surface coverage of all intermediates at ¼ monolayer as an approximation. The Ru (0001) surface were modeled by a four thick metal slab. Periodic slab images in the z-direction were separated by a vacuum layer of 15 Å to avoid spurious interactions between them. All adsorbates and the two topmost slab layers were relaxed by geometry optimization, with forces converged to less than 0.02 eV/Å. Monkhorst-Pack k-points sampling [7] of 4×4×1 were used for all calculations. The zero-point energy corrections for adsorbates [8] was considered for the Gibbs free energies calculations.

Supplementary Tables

Table S1. Contents of Ru in the catalysts determined from the ICP-OES measurements.

Catalyst	Metal mass (wt.%)
Ru/PEI-XC	8.50
Ru/SPEI-XC	8.02
Ru/LPEI-XC	8.00
Ru/XC	8.65

Table S2. Comparison of the Ru/PEI-XC catalyst with some state-of-the-art Ru-based electrocatalysts for HOR in alkaline media.

Electrocatalyst	Electrolyte	ECSA [m^2 g_{metal}^{-1}]	$j_{0,\ ECSA}$ [mA cm_{metal}^{-2}]	$j_{k,\ m}^{50\ mV}$ [A g_{metal}^{-1}]	Loading (μg_{PGM} cm^{-2})	Reference
Ru/PEI-XC	0.1M KOH	19.6	0.687	423.3	21.7	This work
Ru/SPEI-XC	0.1M KOH	17.2	0.627	353.8	20.4	This work
Ru/LPEI-XC	0.1M KOH	16.0	0.673	363.6	20.4	This work
Ru/ XC	0.1 M KOH	20.4	0.332	373.9	22.1	This work
20%Pt/C	0.1 M KOH	56.9	0.200	385.6	20.4	This work
P-Ru/C	0.1 M KOH	56	0.720	--	6.06	[9]
Ru/C-H_2O/ CH_3CH_2OH	0.1 M KOH	47.9	0.650	41.1	180	[10]
$Ru_{2.3}Ni_1$/C	0.1 M KOH	100	--	82	40	[11]
Ru_7Ni_3/C	0.1 M KOH	40	--	9400	0.76 μg_{PGM}	[12]
$Pt_{0.25}Ru_{0.75}$/N-C	0.1 M KOH	117.3	1.410	--	--	[13]
Ru NP/PC	0.1 M KOH	115.45	0.227	--	50.1	[14]
Ru/C (3.1nm)	0.1 M NaOH	131	0.063	--	10	[15]

-- Data unavailable.

Table S3. HER performance Ru/PEI-XC catalyst and state-of-the-art Ru-based electrocatalysts.

Catalyst	Electrolyte	η_{10} (mV vs. RHE)	TOF (s^{-1})	Reference
Ru/PEI-XC	1 M KOH	13	36.30 @$\eta_{100\ mV}$	This work
Ru/SPEI-XC	1 M KOH	16	43.80 @ $\eta_{100\ mV}$	
Ru/LPEI-XC	1 M KOH	16	42.80 @ $\eta_{100\ mV}$	
Ru/ XC	1 M KOH	23	30.81 @ $\eta_{100\ mV}$	
20%Pt/C	1 M KOH	33	2.75 @ $\eta_{100\ mV}$	
P-Ru/C	1 M KOH	31	0.40 @ $\eta_{25\ mV}$	9
Ru/C-H_2O/ CH_3CH_2OH	1 M KOH	53	3.57 @ $\eta_{50\ mV}$	10
Ru NW	1 M KOH	38	3.64 @ $\eta_{20\ mV}$	16
2DPC-RuMo	1 M KOH	18	--	1
RuCu/CQDs-600	1 M KOH	23	--	17
RuCoP	1 M KOH	23	10.95 @ $\eta_{100\ mV}$	18
Ni@Ni_2P-Ru	1 M KOH	41	--	19
Ru@MWCNT	1 M KOH	17	0.22 @ $\eta_{30\ mV}$	20
0.27-RuO_2@C	1 M KOH	20	0.18 @ $\eta_{40\ mV}$	21
RuP (L-RP)	1 M KOH	18	17 @ $\eta_{100\ mV}$	22
Ru@GnP	1 M KOH	22	0.29 @ $\eta_{150\ mV}$	23
PP-Ru/RuO_2-GC	1 M KOH	25	--	24
NiFeRu-LDH	1 M KOH	29	0.68 @ $\eta_{30\ mV}$	25
Ru/C	1 M KOH	24	--	26
4H/fcc Ru NTs	1 M KOH	23	--	27
Ru-NGC	1 M KOH	37	--	28

-- Data unavailable.

Table S4. The electrochemical parameters obtained by fitting the EIS spectra of the Ru/XC and Ru/PEI-XC catalysts in Fig. 5e.

Catalyst	$R_s(\Omega)$	CPE1-T	CPE1-P	$R_{ct}(\Omega)$	CPE2-T	CPE 2-P	$R_m(\Omega)$
Ru/XC	4.5	$3.3*10^{-3}$	0.8	5.0	$2.1*10^{-2}$	0.7	7.1
Ru/PEI-XC	4.8	$7.4*10^{-3}$	0.7	3.1	$1.7*10^{-2}$	0.8	2.6

Supplementary Figures

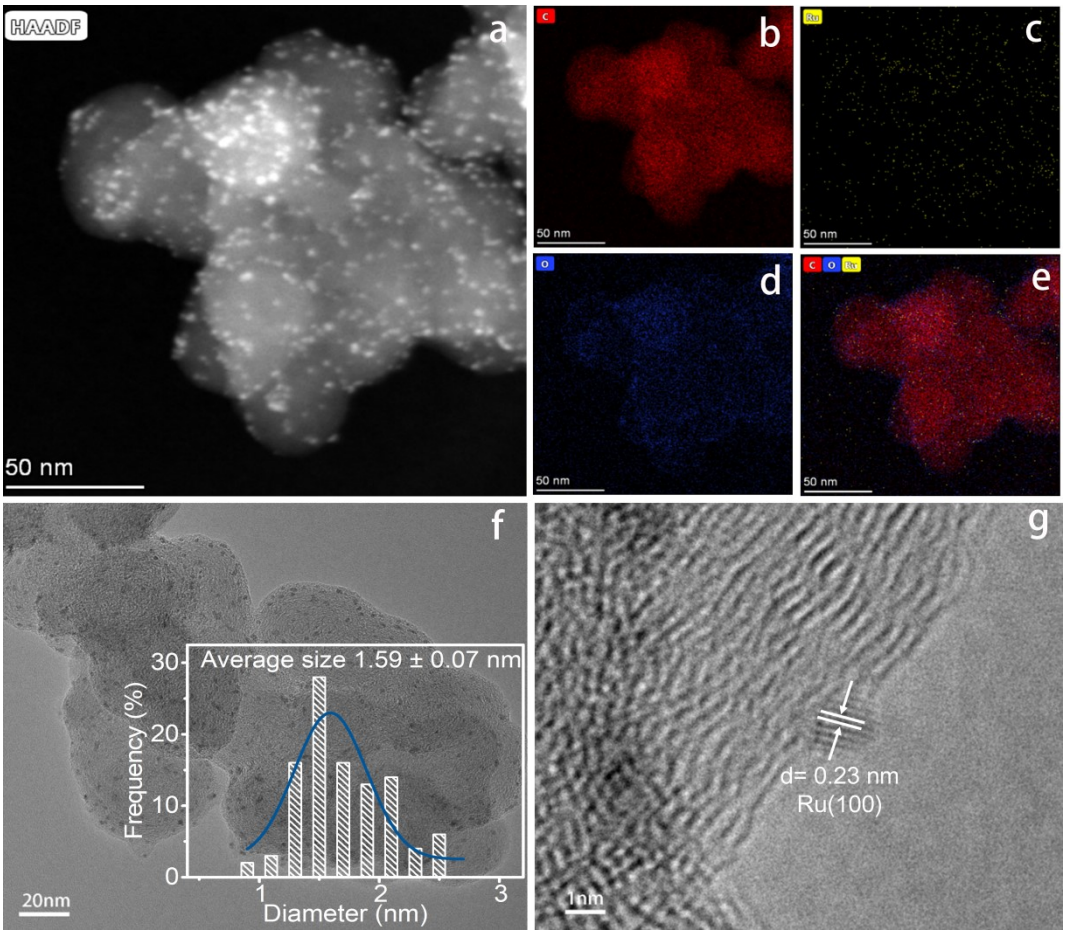

Fig. S1 (a-e) High-angle annular dark-field (HAADF) scanning TEM (STEM) image and corresponding energy-dispersive X-ray spectrometry (EDX) mapping showing the distribution of N, Ru, O and C of a nanoparticle in Ru/ XC. (f) TEM image of Ru/ XC. The inset is the histogram distribution of particle size. (g) HRTEM image of a single particle in Ru/XC.

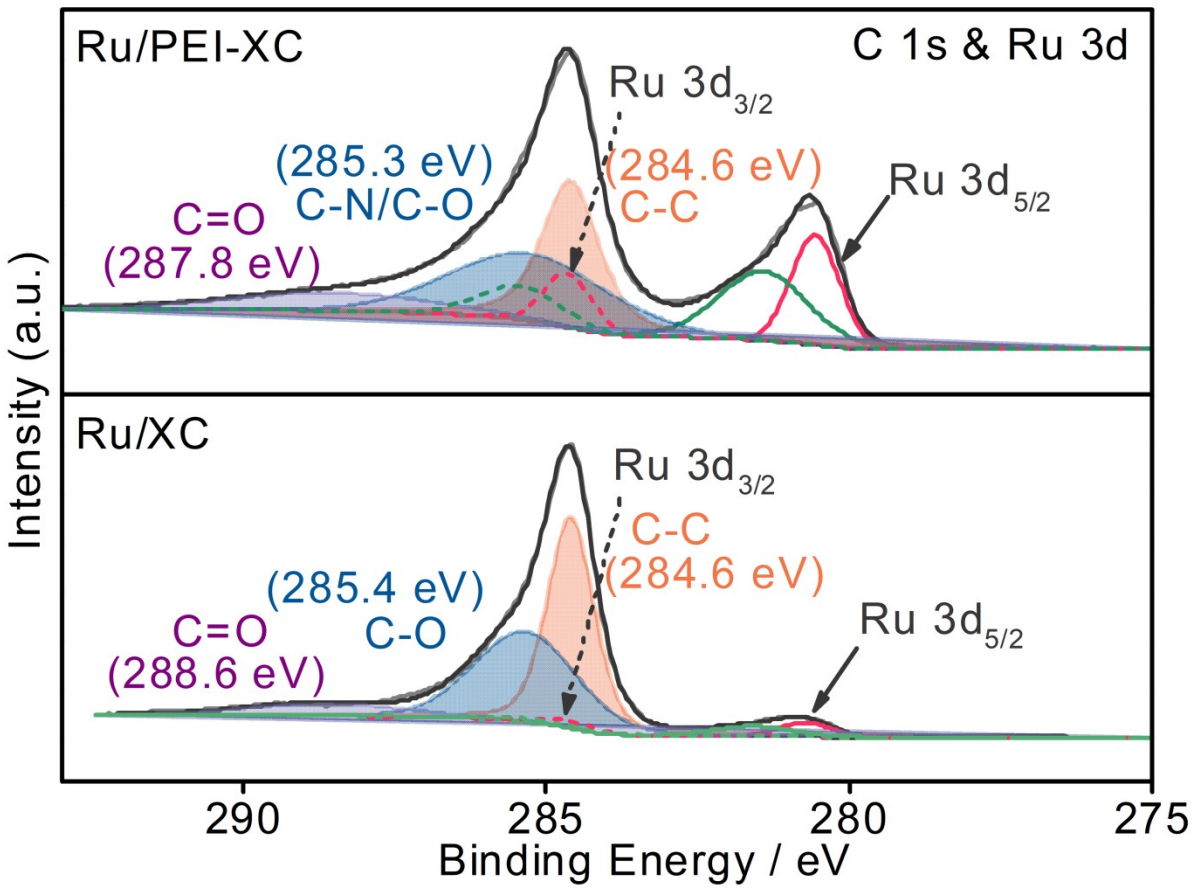

Fig. S2 High resolution C 1s & Ru 3d XPS spectra of Ru/PEI-XC and Ru/XC.

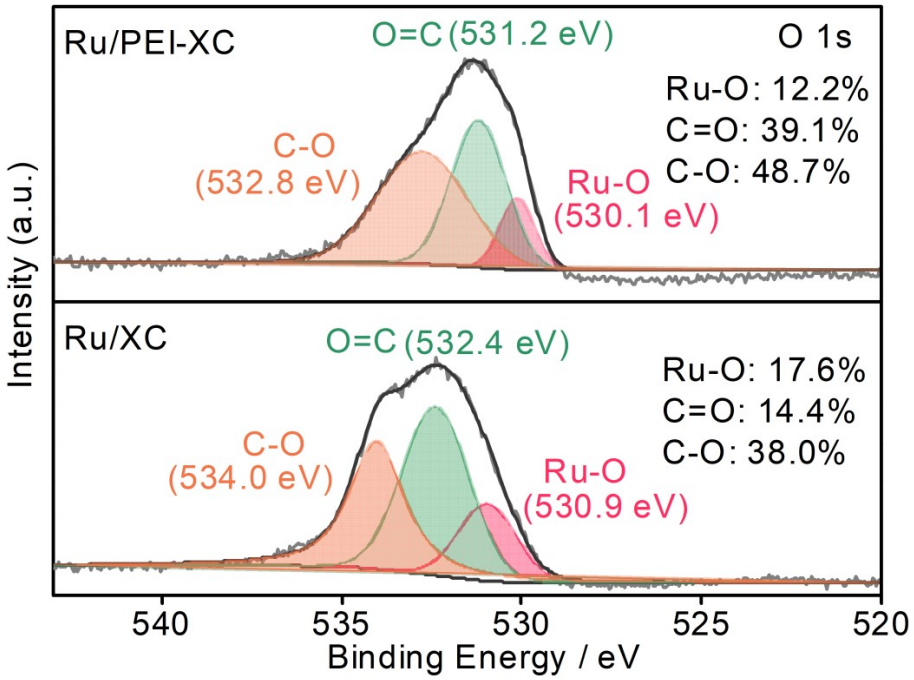

Fig. S3 High resolution O 1s XPS spectra of Ru/PEI-XC and Ru/XC.

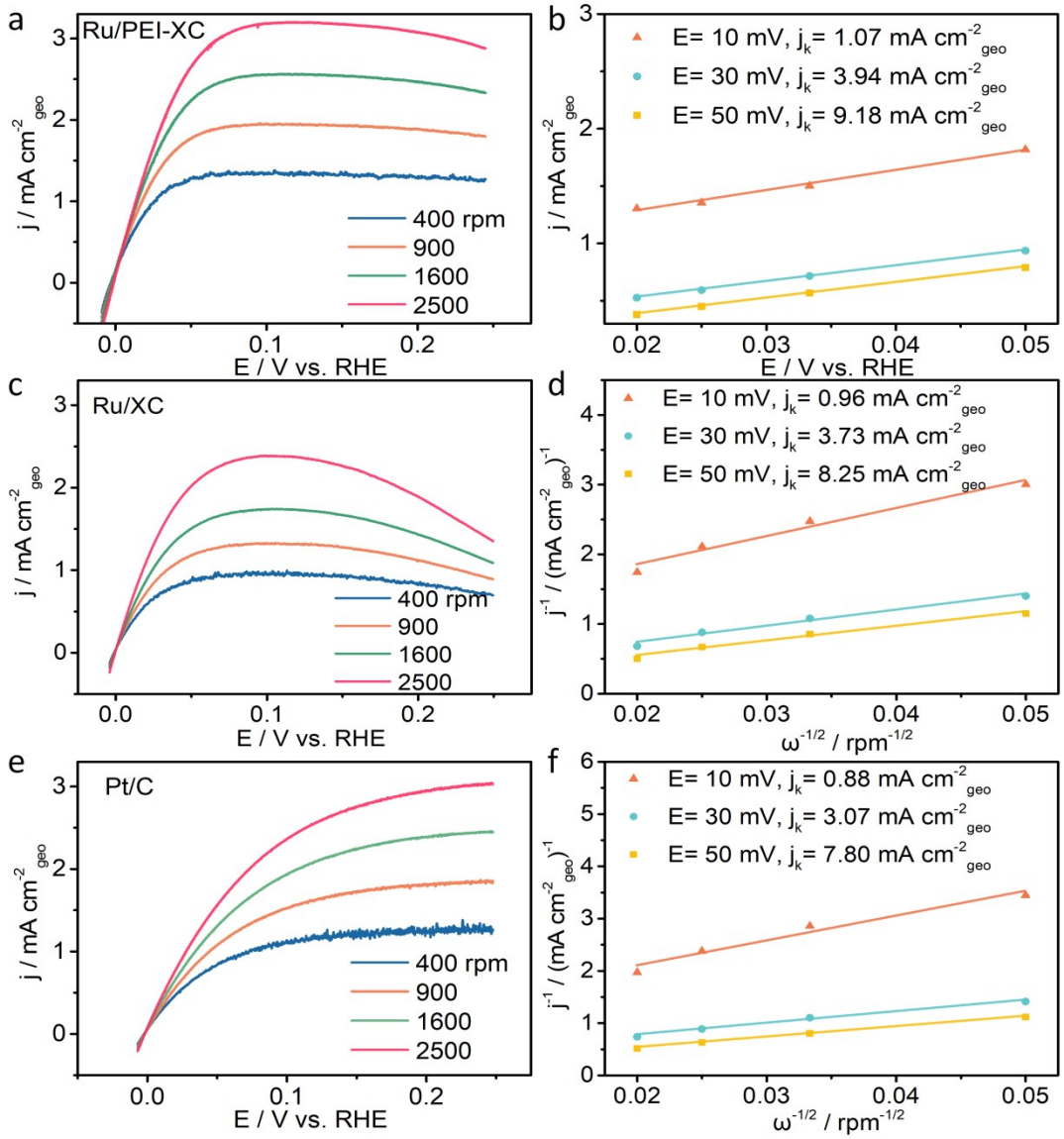

Fig. S4 HOR polarization curves on (a) Ru/PEI-XC, (c) Ru/XC and (e) Pt/C at different rotating rates in H_2-saturated 0.1 M KOH electrolyte, and (b, d, f) the corresponding K-L plots at different potentials. Scan rate: 1 mV s^{-1}.

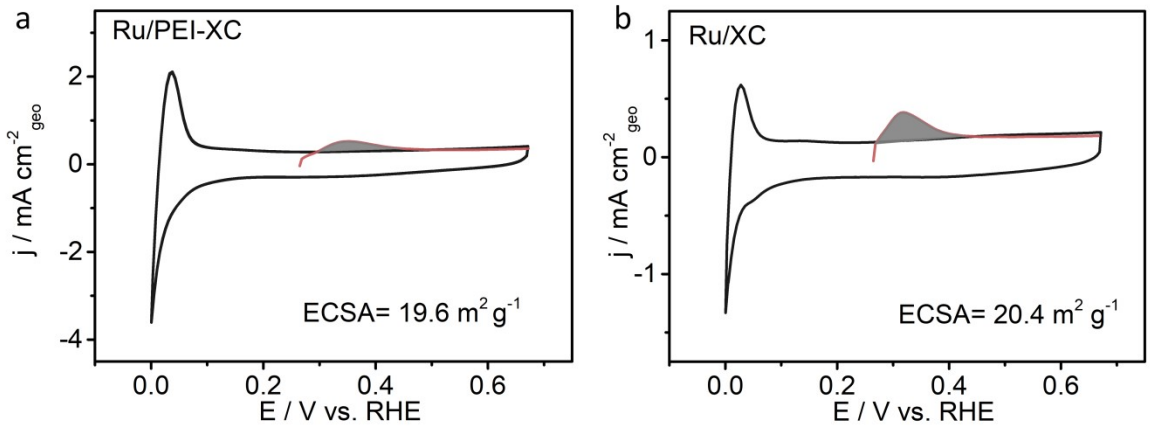

Fig. S5 (a)The Cu_{upd} stripping voltammograms in 0.5 M H_2SO_4 with 5 mM of $CuSO_4$ on Ru/PEI-XC and (b) Ru/XC. The black curve was obtained in 0.5 M H_2SO_4 without $CuSO_4$.

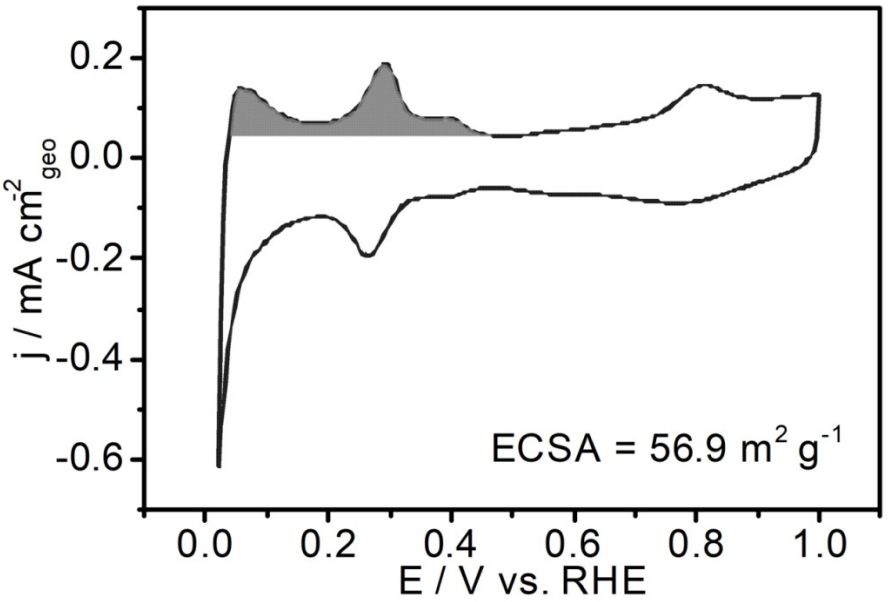

Fig. S6 CV of Pt/C in N_2-saturated 0.1 M KOH at a scanning rate of 10 mV s^{-1}. The catalyst loading on the electrode is 20.4 $\mu g_{Pt}\,cm^{-2}$.

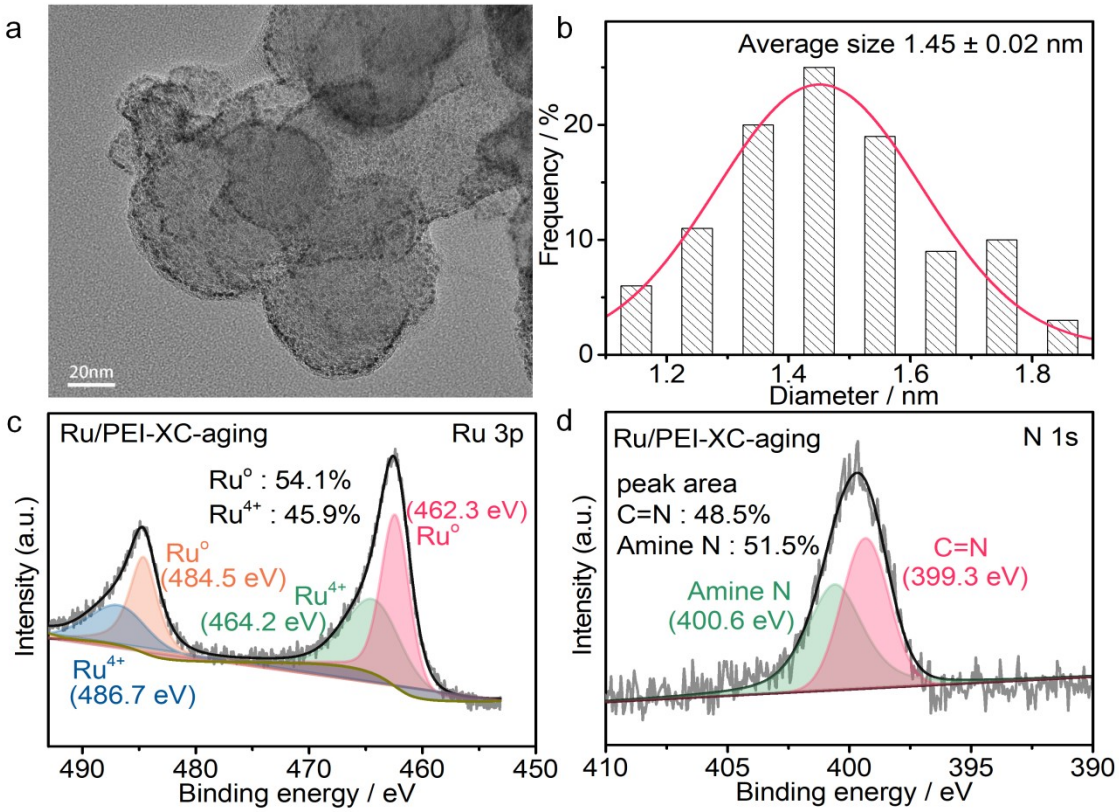

Fig. S7 (a) TEM images and (b) the corresponding particle size distribution of Ru/PEI-XC after ADT (denoted as Ru/PEI-XC-aging). (c) High-resolution Ru 3p and (d) N 1s XPS spectra of Ru/PEI-XC-aging.

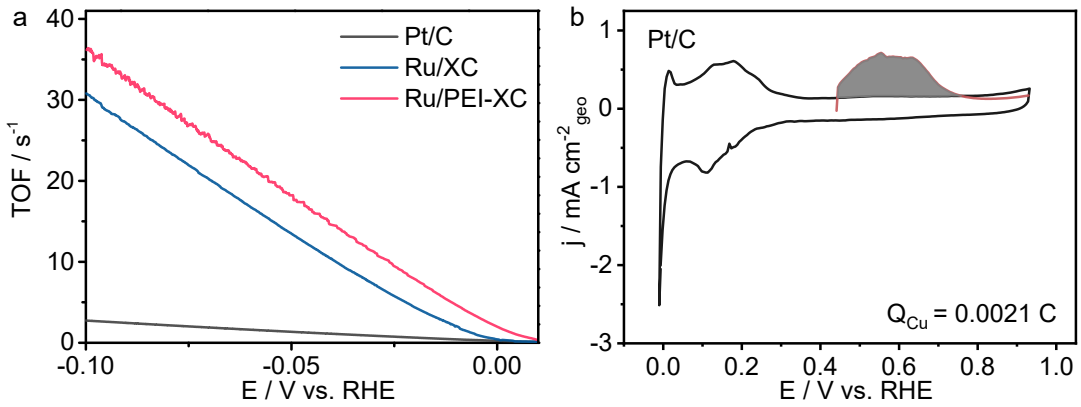

Fig. S8 (a) The potential-dependent TOF curves of Ru/PEI-XC, Ru/XC and Pt/C derived from Fig. 5a. (b) The Cu_{upd} stripping voltammograms in 0.5 M H_2SO_4 with 5 mM of $CuSO_4$ on Pt/C catalyst. The black curve was obtained in 0.5 M H_2SO_4 without $CuSO_4$. The catalyst loading is kept the same with that in HER tests, 255μg $_{cat}$ cm^{-2}_{geo}.

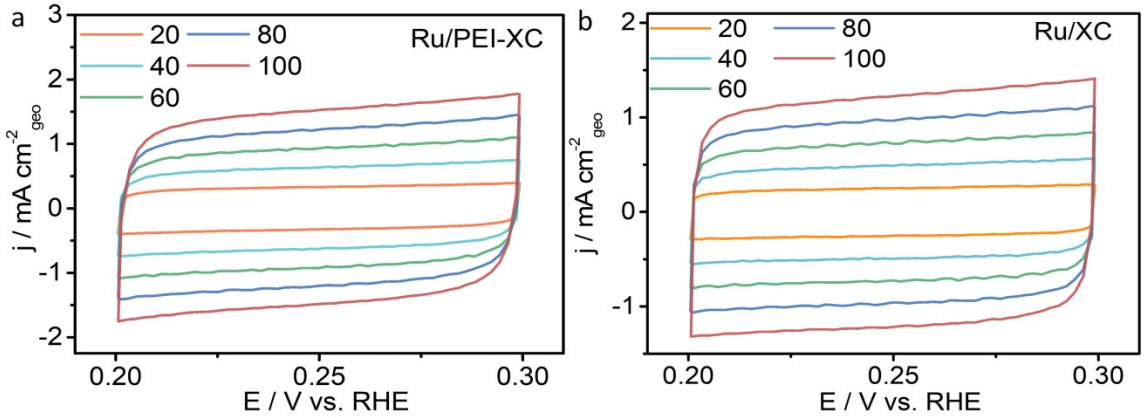

Fig. S9 CV of **(**a)Ru/PEI-XC and (b) Ru/XC in N_2-saturated 1 M KOH at different scanning rates. The unit of the scanning rate is mV s^{-1}.

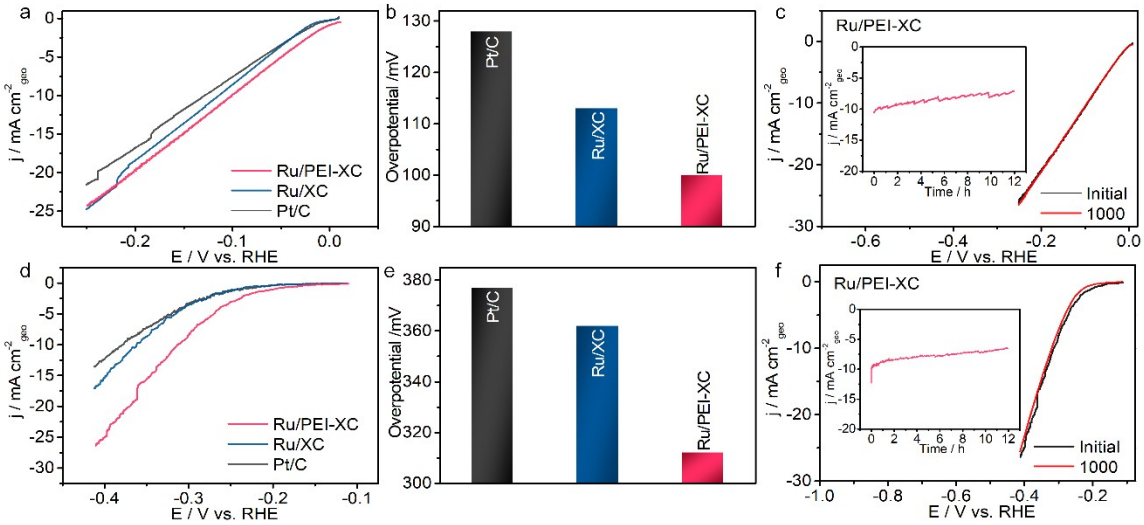

Fig. S10 HER performance in N_2-saturated 0.1 M KOH and 0.6 M NaCl electrolyte. (a, d) HER polarization curves. (b, e) Overpotential at -10 mA cm^{-2}. (c, f) HER polarization curves initial and after 1000 cycles. The insert is the chronoamperometry curve recorded at 0.1 V vs. RHE.

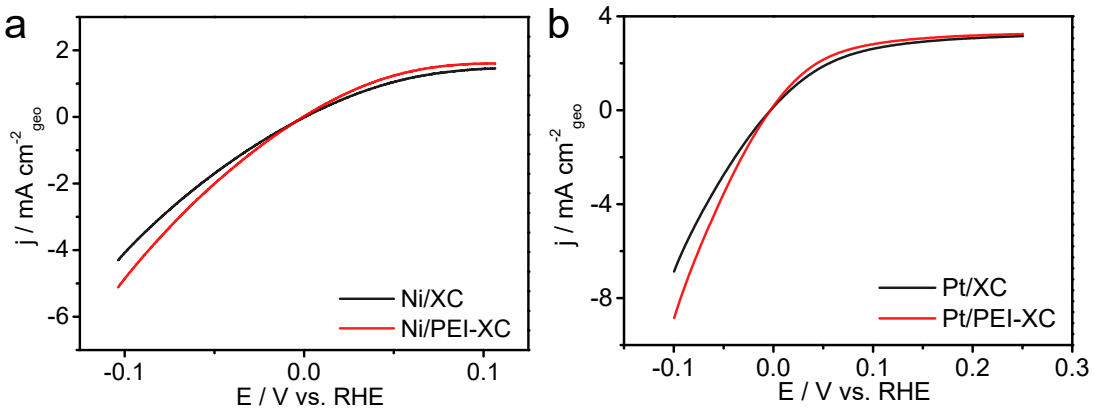

Fig. S11 (a) HOR/HER polarization curves of Ni/XC and Ni/PEI-XC. (b) HOR/HER polarization curves of Pt/XC and Pt/PEI-XC. The scan rate is 1 mV s^{-1} and the rotating rate of 2500 rpm.

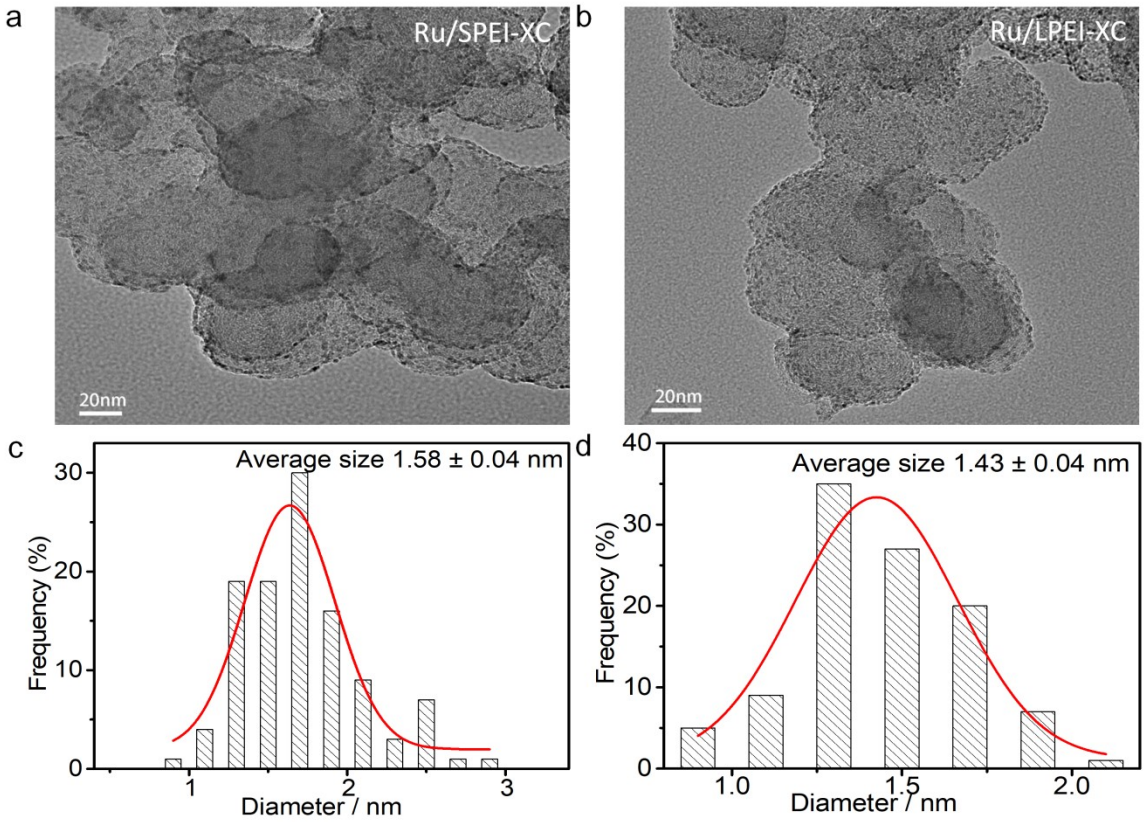

Fig. S12 (a, c) TEM images and the corresponding particle size distribution of Ru/SPEI-XC and (b, d) Ru/LPEI-XC.

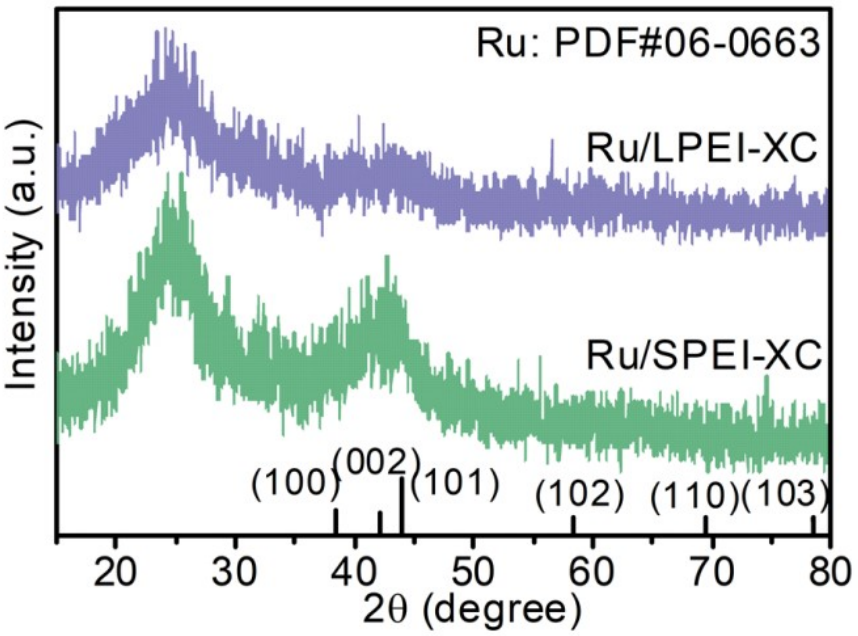

Fig. S13 XRD patterns of Ru/SPEI-XC and Ru/LPEI-XC.

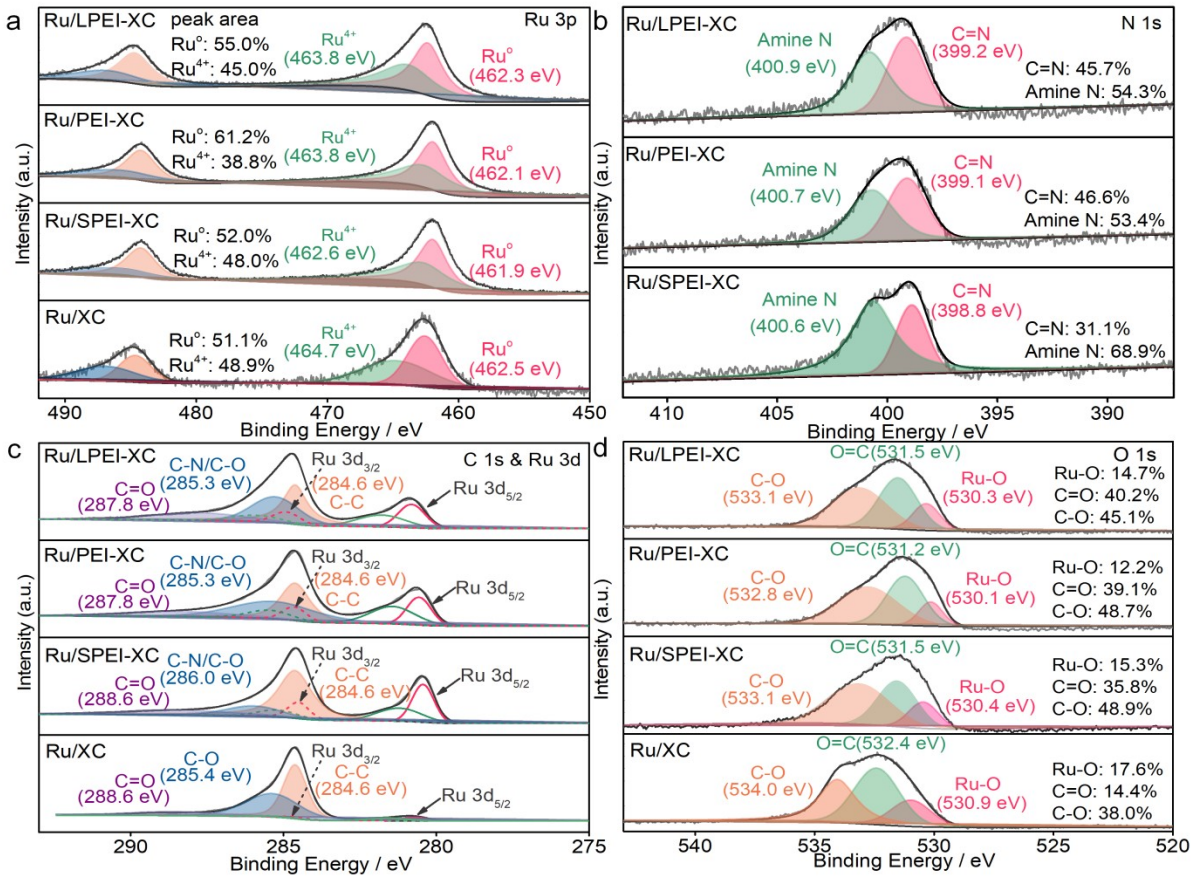

Fig. S14 (a) High-resolution Ru 3p, (c) C 1s&Ru 3d and (d) O 1s XPS spectra of Ru/PEI-XC, Ru/SPEI-XC, Ru/LPEI-XC and Ru/XC. (b) High-resolution N 1s XPS spectra of Ru/PEI-XC, Ru/SPEI-XC and Ru/LPEI-XC.

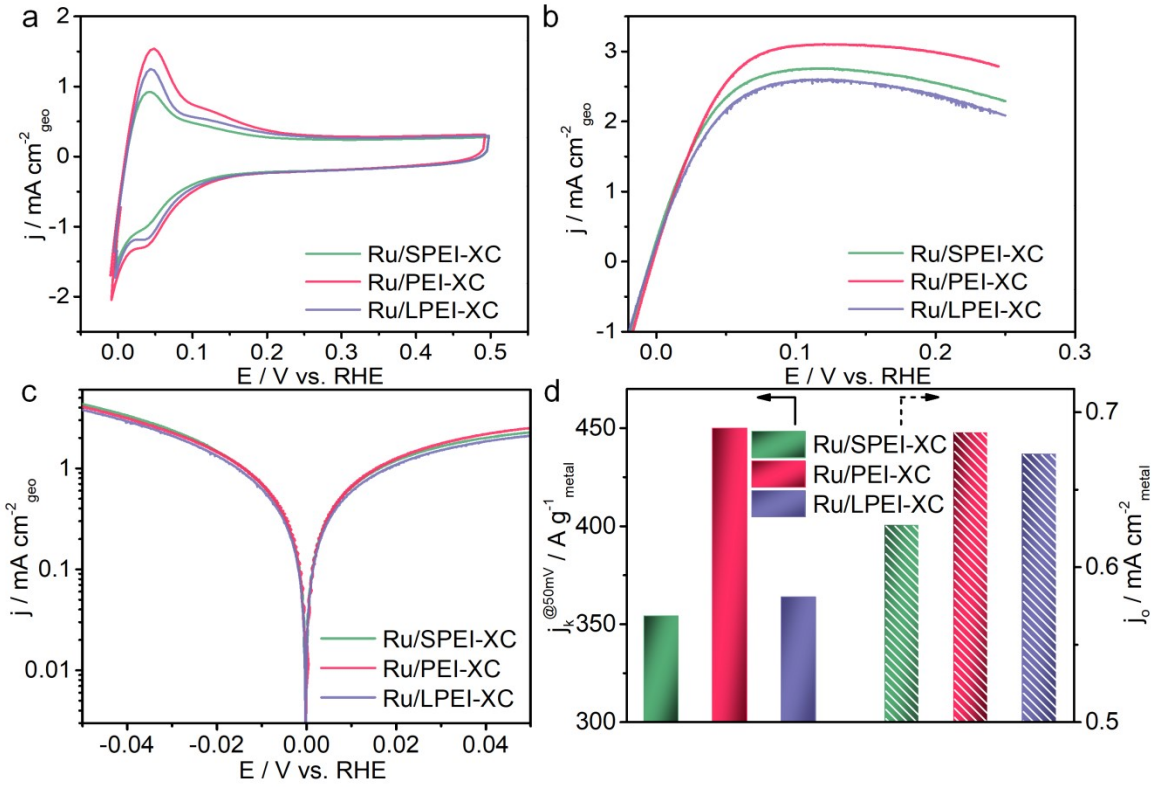

Fig. S15 (a) CV curves of Ru/PEI-XC, Ru/SPEI-XC and Ru/LPEI-XC in N_2-saturated 0.1 M KOH. The scan rate is 10 mV s^{-1}. (b) HOR polarization curves of Ru/PEI-XC, Ru/SPEI-XC and Ru/LPEI-XC in H_2-saturated 0.1M KOH. The scan rate is 1 mV s^{-1}. (c) Tafel plots and (d) the kinetic activity at 50 mV and mass activity of Ru/PEI-XC, Ru/SPEI-XC and Ru/LPEI-XC.

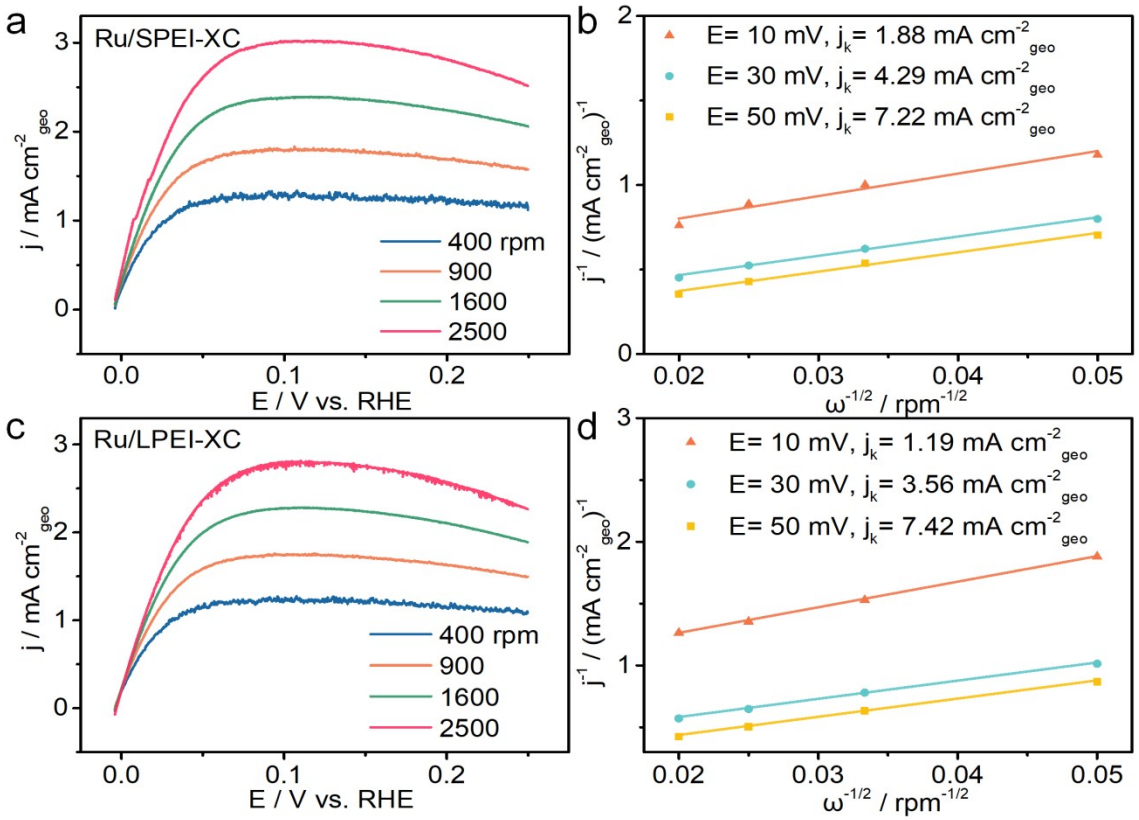

Fig. S16 HOR polarization curves on (a) Ru/SPEI-XC and (c) Ru/LPEI-XC at different rotating rates in H_2-saturated 0.1 M KOH electrolyte, and (b, d) the corresponding K-L plots at different potentials. Scan rate: 1 mV s^{-1}.

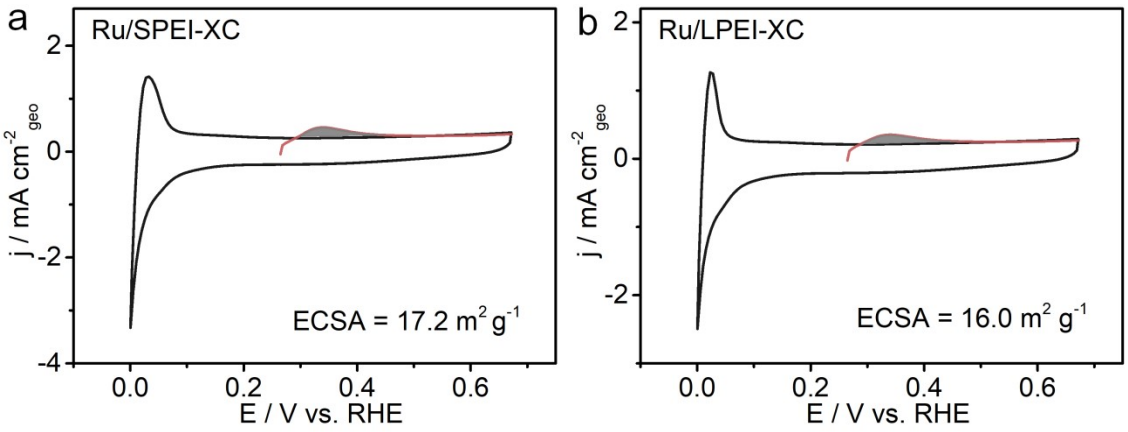

Fig. S17 (a)The Cu_{upd} stripping voltammograms in 0.5 M H_2SO_4 with 5 mM of $CuSO_4$ on Ru/SPEI-XC and (b) Ru/SPEI-XC. The black curve was obtained in 0.5 M H_2SO_4 without $CuSO_4$.

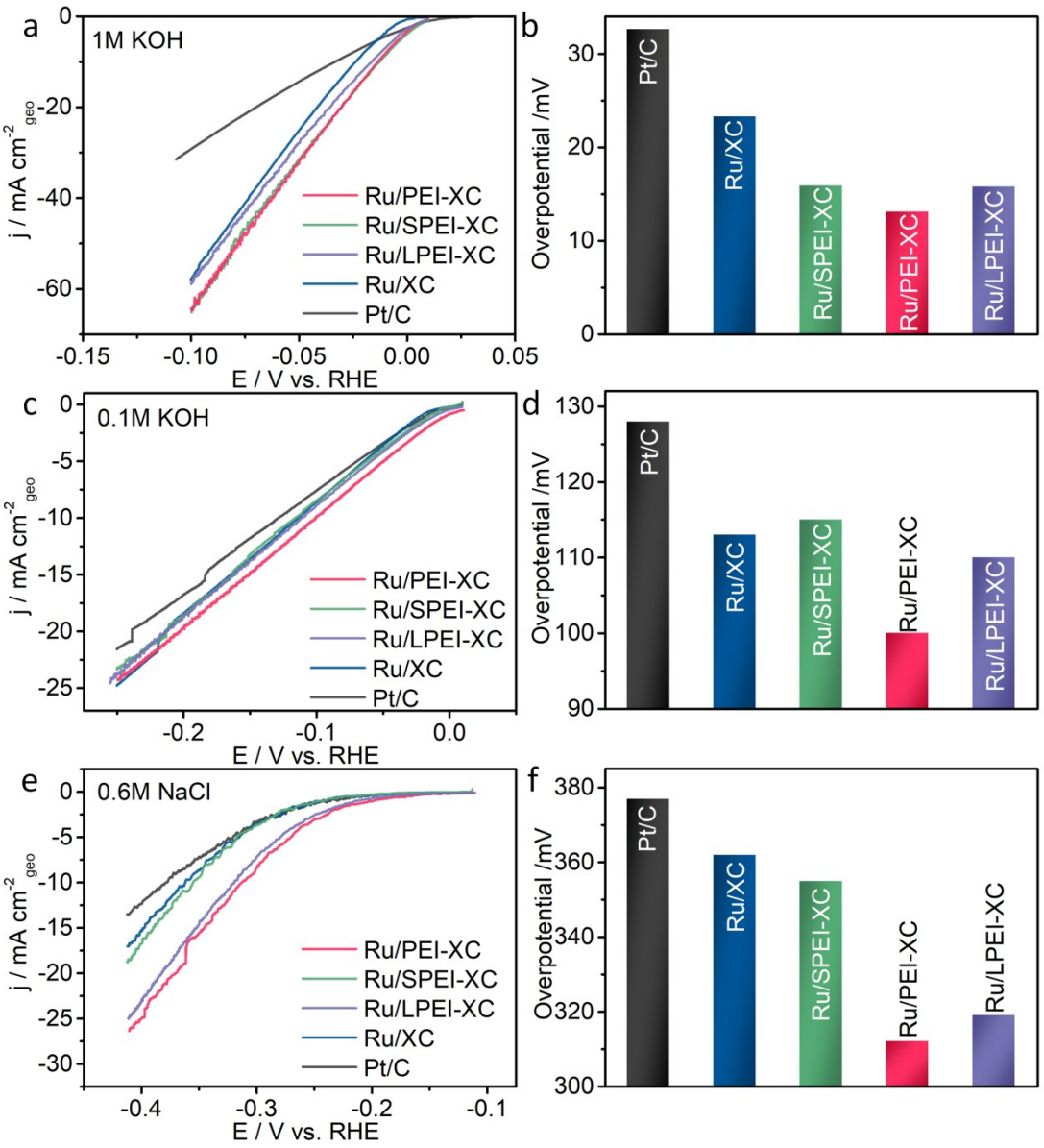

Fig. S18 HER performance in different electrolytes. (a) HER polarization curves in N_2-saturated 1 M KOH electrolyte and (b) the Overpotential at -10 mA cm^{-2}. (c) HER polarization curves in N_2-saturated 0.1 M KOH electrolyte and (d) the Overpotential at -10 mA cm^{-2}. (e) HER polarization curves in N_2-saturated 0.6 M NaCl electrolyte and (f) the overpotential at -10 mA cm^{-2}.

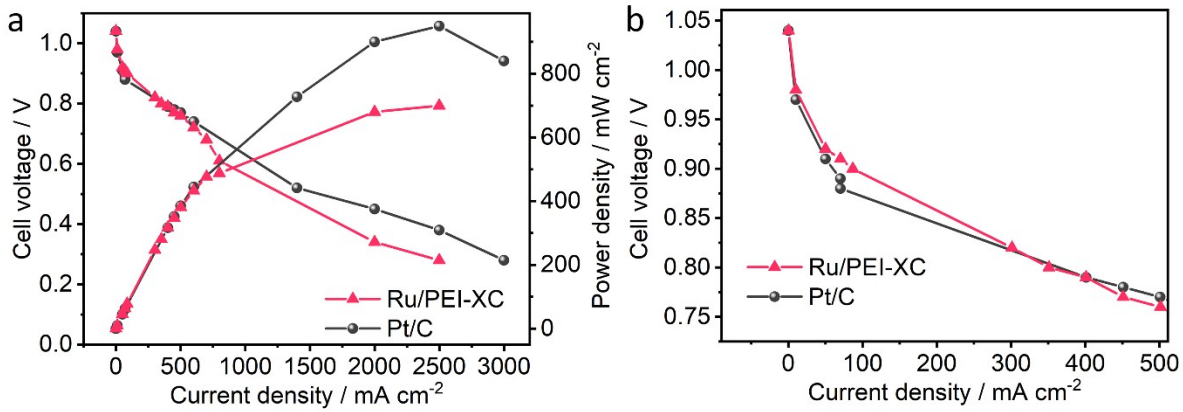

Fig. S19 (a) Discharging curves of the AEMFCs with Ru/PEI-XC and Pt/C as the anode catalyst. (b) The enlarged discharging curves at the low polarization region in (a). Anode metal loading： 0.1 mg_{Ru} cm^{-2}, 0.2 mg_{Pt} cm^{-2}; Cathode metal loading: 0.4 mg_{Pt} cm^{-2}. The cell is operated at 80°C. The anode is fed with 100% humidified H_2 at 2000 mL min^{-1},100% RH. The cathode is fed with 100% humidified O_2 at 1000 mL min^{-1}. The backpressure of both sides is 200 kPa.

References

1 K. Tu, D. Tranca, F. Rodriguez-Hernandez, K. Jiang, S. Huang, Q. Zheng, M. X. Chen, C. Lu, Y. Su, Z. Chen, H. Mao, C. Yang, J. Jiang, H. W. Liang and X. Zhuang, *Adv. Mater.*, 2020, **32**, e2005433.

2 X. Wu, Z. Wang, D. Zhang, Y. Qin, M. Wang, Y. Han, T. Zhan, B. Yang, S. Li, J. Lai and L. Wang, *Nat. Commun.*, 2021, **12**, 4018.

3 P. E. Blöchl, *Phys. Rev. B*, 1994, **50**, 17953-17979.

4 J. P. Perdew, K. Burke and M. Ernzerhof, *Phys. Rev. Lett.*, 1996, **77**, 3865-3868.

5 G. Kresse and J. Hafner, *Phys. Rev. B*, 1993, **47**, 558-561.

6 G. Kresse and J. Furthmüller, *Phys. Rev. B*, 1996, **54**, 11169-11186.

7 H. J. Monkhorst and J. D. Pack, *Phys. Rev. B*, 1976, **13**, 5188-5192.

8 J. K. Nørskov, T. Bligaard, A. Logadottir, J. R. Kitchin, J. G. Chen, S. Pandelov and U. Stimming, *J. Electrochem. Soc.*, 2005, **152**, J23.

9 Y. Zhao, X. Wang, G. Cheng and W. Luo, *ACS Catal.*, 2020, **10**, 11751-11757.

10 Y. Li, J. Abbott, Y. Sun, J. Sun, Y. Du, X. Han, G. Wu and P. Xu, *Appl. Catal. B*, 2019, **258**, 117952.

11 C.-P. Huang, M.-C. Tsai, X.-M. Wang, H.-S. Cheng, Y.-H. Mao, C.-J. Pan, J.-N. Lin, L.-D. Tsai, T.-S. Chan, W.-N. Su and B.-J. Hwang, *Catalysis Science & Technology*, 2020, **10**, 893-903.

12 Y. Xue, L. Shi, X. Liu, J. Fang, X. Wang, B. P. Setzler, W. Zhu, Y. Yan and Z. Zhuang, *Nat. Commun.*, 2020, **11**, 5651.

13 Y. Cong, C. Chai, X. Zhao, B. Yi and Y. Song, *Adv. Mater. Interfaces*, 2020, **7**, 2000310.

14 M. Ming, Y. Zhang, C. He, L. Zhao, S. Niu, G. Fan and J. S. Hu, *Small*, 2019, **15**, e1903057.

15 J. Ohyama, T. Sato, Y. Yamamoto, S. Arai and A. Satsuma, *J. Am. Chem. Soc.*, 2013, **135**, 8016-8021.

16 J. Yang, Y. J. Ji, Q. Shao, N. Zhang, Y. Y. Li and X. Q. Huang, *Adv. Funct. Mater.*, 2018, **28**, 1803722.

17 Y. Liu, X. Li, Q. Zhang, W. Li, Y. Xie, H. Liu, L. Shang, Z. Liu, Z. Chen, L. Gu, Z. Tang, T. Zhang and S. Lu, *Angew. Chem. Int. Ed.*, 2020, **59**, 1718-1726.

18 J. Y. Xu, T. F. Liu, J. J. Li, B. Li, Y. F. Liu, B. S. Zhang, D. H. Xiong, I. Amorim, W. Li and L. F. Liu, *Energy Environ. Sci.*, 2018, **11**, 1819-1827.

19 Y. Liu, S. L. Liu, Y. Wang, Q. H. Zhang, L. Gu, S. C. Zhao, D. D. Xu, Y. F. Li, J. C. Bao and Z. H. Dai, *J. Am. Chem. Soc.*, 2018, **140**, 2731-2734.

20 D. H. Kweon, M. S. Okyay, S. J. Kim, J. P. Jeon, H. J. Noh, N. Park, J. Mahmood and J. B. Baek, *Nat. Commun.*, 2020, **11**, 1278.

21 H. S. Park, J. Yang, M. K. Cho, Y. Lee, S. Cho, S. D. Yim, B. S. Kim, J. H. Jang and H. K. Song, *Nano Energy*, 2019, **55**, 49-58.

22 J. Yu, Y. N. Guo, S. X. She, S. S. Miao, M. Ni, W. Zhou, M. L. Liu and Z. P. Shao, *Adv. Mater.*, 2018, **30**, 1800047.

23 F. Li, G. F. Han, H. J. Noh, I. Ahmad, I. Y. Jeon and J. B. Baek, *Adv. Mater.*, 2018, **30**, 1803676.

24 J. Creus, S. Drouet, S. Surinach, P. Lecante, V. Colliere, R. Poteau, K. Philippot, J. Garcia-Anton and X. Sala, *Acs Catal.*, 2018, **8**, 11094-11102.

25 G. B. Chen, T. Wang, J. Zhang, P. Liu, H. J. Sun, X. D. Zhuang, M. W. Chen and X. L. Feng, *Adv. Mater.*, 2018, **30**, 1706279.

26 Q. Wang, M. Ming, S. Niu, Y. Zhang, G. Y. Fan and J. S. Hu, *Adv. Energy Mater.*, 2018, **8**, 1801698.

27 Q. P. Lu, A. L. Wang, H. F. Cheng, Y. Gong, Q. B. Yun, N. L. Yang, B. Li, B. Chen, Q. H. Zhang, Y. Zong, L. Gu and H. Zhang, *Small*, 2018, **14**, 1801090.

28 Q. Song, X. Z. Qiao, L. Z. Liu, Z. J. Xue, C. H. Huang and T. Wang, *Chem. Commun.*, 2019, **55**, 965-968.